Macromolecules

pubs.acs.org/Macromolecules Article

Mechanism of Escape of a Single Chain from a Diblock Copolymer Micelle

Sarah C. Seeger, Timothy P. Lodge,* and Kevin D. Dorfman*

Cite This: https://doi.org/10.1021/acs.macromol.2c01742 Read Online

ACCESS | Metrics & More | Article Recommendations | Supporting Information

ABSTRACT: We investigate the dependence of the free energy trajectory for chain expulsion from a diblock copolymer micelle in a selective solvent on core chain length through dissipative particle dynamics simulations and umbrella sampling. The free energy barrier scales linearly with the core block length of the expelled tracer chain for N_{core} = 4−12, consistent with experiments. The simulations further reveal that the core chain undergoes a "hyperstretching" mechanism near the transition state, where the core block partially stretches through the corona to allow monomers further from the chain junction to remain shielded in the micelle core. As the junction extends past the transition state, it becomes more favorable for the chain to be fully expelled, and the monomer furthest from the junction exits the micelle core, allowing the core block to escape from the micelle and collapse upon entering the solvent. We propose a simple model to describe this process of chain expulsion, which provides an effective description of the simulation results.

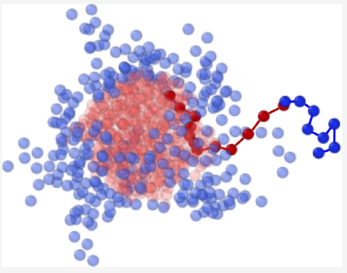

INTRODUCTION

Block copolymers (BCPs) in a selective solvent undergo dynamic self-assembly to form micelles. BCP micelles find use in applications such as nanolithography,[1,2] nanoreactors,[3] oil-based lubrication,[4,5] and vehicles for drug delivery.[6−8] These applications depend on the micelle size, which controls solution properties such as viscosity. Moreover, the release of cargo at the desired time and location, governed by the kinetic stability of the micelles, dictates their success as drug delivery and gene therapy vehicles.[9] Thus, engineering applications of micelles require understanding the relations among BCP variables, micelle size, and relaxation kinetics.

As recently reviewed,[10] micelle relaxation was first described by the Aniansson−Wall model in the context of surfactant systems.[11] This model predicts that micelles equilibrate by a combination of single chain exchange, fusion, and fragmentation. Although these relaxation processes occur on subsecond time scales for surfactant micelles, longer chain lengths result in much slower kinetics for BCPs, often from seconds to days, or on even longer time scales for "frozen" systems.[12−14] Importantly, chain exchange is generally designated the "fast" process, as it has the lowest activation energy for systems close to equilibrium.[15,16] In particular, single chain exchange dominates for spherical micelles close to the equilibrium aggregation number, Q_{eq}. Despite extensive work toward understanding the kinetics of single chain exchange, the dependence of the escape time on the chain size, particularly the core block length N_{core}, is not well understood.

Chain exchange in BCPs has been explored experimentally using techniques such as time-resolved small-angle neutron scattering (TR-SANS),[17−28] nonradiative energy transfer,[29,30] and fluorescence.[31−34] Particularly, the kinetics of chain exchange near equilibrium have been quantified using TR-SANS. In this experiment, a solution of micelles prepared with a standard (hydrogenated) core block is mixed with a second solution prepared with their perdeuterated counterpart in a zero-average-contrast solvent. Initially, scattering is at a maximum. As chains are exchanged between micelles the chains will become randomly dispersed, and the scattering intensity decays to zero. Fitting the relaxation function of the scattering intensity over time yields a characteristic exchange time τ_{ex}. The free energy barrier to chain exchange is extracted by fitting to $\tau_{ex} = \tau_0 \exp(E_a/k_BT)$ using a series of different temperatures. Through this method, it is then possible to obtain information about the free energy barrier to chain exchange, which is assumed to be dominated by the expulsion of the core block from the micelle core.

Although TR-SANS provides an estimate of the free energy barrier to chain exchange, it is unable to resolve the conformation of the core block upon expulsion. Importantly, the N_{core} dependence of the relaxation time for single chain exchange must depend on this transition state. Experiments have been interpreted in the context of the Halperin and Alexander model.[15] This theory assumes that as the core block of a chain undergoing expulsion moves from the dry micelle core into the solvated corona, it forms a collapsed globule with radius of gyration $R_g \sim N_{core}^{1/3}$ at the transition state. The application of Kramers' theory thus leads to a free energy

Received: August 21, 2022
Revised: October 15, 2022

barrier to expulsion that scales with the surface area of that globule, $N_{core}^{2/3}$. However, extensive TR-SANS work probing the effect of the core block length on the chain exchange rate has revealed that the barrier to chain exchange increases *linearly* with N_{core},[17,18,20] a scaling also consistently observed for self-diffusion of BCPs in melts.[35−37] This important experimental result is inconsistent with the scaling prediction of the Halperin and Alexander theory and has brought into question the assumptions of the model, particularly the conformation of the core block upon expulsion.

Recently,[38] we have shown that the full free energy profile of chain expulsion can be computed by combining dissipative particle dynamics simulations (DPD)[39−47] with an umbrella sampling technique.[48] A similar approach has been applied to surfactant systems to access the free energy barrier for expulsion.[49−51] For an isolated micelle of A_4B_8 chains in a dilute solution, where the A block forms the core, the free energy barrier to chain exchange was found to increase linearly with DPD excess interaction energy Δa (analogous to a simulation interaction parameter χ).[38] In the strong segregation limit, the transition state involved deformation of the spherical micelle core to minimize unfavorable core block contacts.[38] Contrary to the Halperin and Alexander model,[15] these initial observations suggested a *stretched* conformation of the core block upon expulsion at the transition state for a micelle of A_4B_8 chains in a dilute solution. Compared to past approaches to study chain exchange, this technique provides direct access to the transition state for chain expulsion.[38]

Here we extend this method to obtain a scaling of the free energy barrier to expulsion with N_{core}. We analyze the effect of core block length using a tracer chain in a micelle of otherwise constant composition to assess the postulated transition state to chain exchange. Additionally, we examine the effect of changing N_{core} of the other chains constituting the micelle to assess the effect of micelle size independently from the length of the tracer core block, as previously it has not been possible to distinguish between N_{core} of the expelled chain and N_{core} of the micelle. Notably, the simulations reveal a transition state that is consistent with the linear scaling in N_{core} observed in past experiments[16,17,19] and suggest a partial "hyperstretching" mechanism,[52] whereby the terminal core block monomer remains in the core until the rest of the core block is significantly stretched. At the transition state, the last monomer departs the core, only then allowing the core block to collapse to a globular state.

■ SIMULATION METHODOLOGY

DPD simulations of dilute BCP solutions were performed in LAMMPS using the method recently outlined in Seeger et al.[38] Similar to past DPD work,[38,41,42] diblocks are modeled by coarse-grained polymers of A_xB_8, where x is the number of solvophobic A beads (here, x ranges from 4 to 12). Monomer beads of mass m are held together by harmonic bonds with $\mathbf{F}^{bond} = k\,(r_{ij} - r_0)\hat{\mathbf{r}}_{ij}$, where the force constant $k = 100k_BT/d_p^2$ in terms of the DPD length scale d_p, k_B is Boltzmann's constant, T is temperature, and $r_0 = d_p$. $\hat{\mathbf{r}}_{ij}$ is the (dimensionless) unit vector between particles i and j, where $\mathbf{r}_{ij} = \mathbf{r}_i - \mathbf{r}_j$ is the distance vector and r_{ij} is its magnitude. The solvent S was modeled by single beads of the soluble (B) block in the BCP chain. The repulsive force between any two beads is taken as the pairwise sum of a conservative force, $\mathbf{F}^C$, a random force $\mathbf{F}^R$ that captures the thermal fluctuations, and a frictional force $\mathbf{F}^D$ that dissipates energy to conserve the total system energy[39,40]

$$\mathbf{F}_{ij} = \mathbf{F}_{ij}^{C} + \mathbf{F}_{ij}^{R} + \mathbf{F}_{ij}^{D} \quad (1)$$

where

$$\mathbf{F}_{ij}^{C} = -[a_{ij}(r_c - r_{ij})]\hat{\mathbf{r}}_{ij} \quad (2)$$

$$\mathbf{F}_{ij}^{R} = \sigma w^{R}\theta_{ij}\Delta t^{-1/2}\hat{\mathbf{r}}_{ij} \quad (3)$$

$$\mathbf{F}_{ij}^{D} = -\xi w^{D}(\hat{\mathbf{r}}_{ij}\cdot\mathbf{v}_{ij})\hat{\mathbf{r}}_{ij} \quad (4)$$

for $r_{ij} < r_c$.[39,40] All forces are short-ranged with a cutoff distance $r_c = d_p$. Analogous to $\mathbf{r}_{ij}$, $\mathbf{v}_{ij}$ is the velocity vector between the two particles, $w^D = (w^R)^2 = (1 - r_{ij}/r_c)^2$,[40] and θ_{ij} is a Gaussian random number with zero mean and unit variance. The dissipative force has a friction coefficient $\xi = 3.0(mk_BT/d_p^2)^{1/2}$, and the random force has a noise amplitude $\sigma = (2\xi k_BT)^{1/2}$. A time step of $\Delta t = 0.04(md_p^2/k_BT)^{1/2}$ was used.[40,41] In all simulations, the repulsive interaction energy for the conservative force $a_{AA} = a_{BB} = a_{BS}$ was set to $25k_BT/d_p^2$ for like particles. For core block and corona/solvent contacts (A−B and A−S), the excess interaction energy $\Delta a = a_{AB} - a_{AA}$ was set to $25k_BT/d_p^2$, corresponding to the strong segregation regime.[38] Notably, k_BT and d_p are the DPD units for energy and distance, respectively. In the following, we omit units for simplicity.

To create the micelles, 81000 beads including 35 chains of A_xB_8 and one chain of A_yB_8 (x and y = 4, 6, 8, 12) were initialized randomly in a cubic box with side 30; periodic boundary conditions were applied.[41,42] To initialize the simulation, a harmonic biasing potential was applied to the core blocks to prepare a single micelle of aggregation number Q = 36, as was used in previous work for an A_4B_8 system.[38] The biasing potential is removed, and the micelle is allowed to relax for $t \approx 10^5$ steps prior to the production run. Importantly, the choice Δa = 25 effectively halts chain exchange in this system, such that the micelle is stable and no chains leave this micelle prior to the umbrella sampling procedure. The micelle in these simulations is thus frozen at the chosen Q and is not at the global equilibrium; however, we note that many experimental systems are also out of equilibrium due to the extremely long exchange time scales.[14,14] Moreover, because this work probes single-chain behavior rather than a system ensemble, a detailed analysis of Q_{eq} was not deemed necessary. We do note that the extent of corona crowding may be different based on the number of core beads x chosen for the simulation; however, the influence of the corona-forming block length is more subtle compared to the core-forming block,[53−55] and a detailed study remains a topic for future work.

A single A_yB_8 chain, denoted the "tracer", was selected from the locally equilibrated micelle. To perform umbrella sampling, we defined a reaction coordinate r as the distance between the center-of-mass of the micelle and the position of the AB chain junction for the designated tracer chain, following Halperin and Alexander.[15] A harmonic force with k = 12.0 was then applied to bias the reaction coordinate r to fluctuate around the chosen value for each umbrella sampling window, using the LAMMPS[56] *colvars* module for ∼(1−2) × 10^5 time steps. Because another chain leaving the micelle would result in an inaccurate center-of-mass calculation, the trajectory was analyzed to confirm that no additional unimer expulsion

https://doi.org/10.1021/acs.macromol.2c01742
Macromolecules XXXX, XXX, XXX−XXX

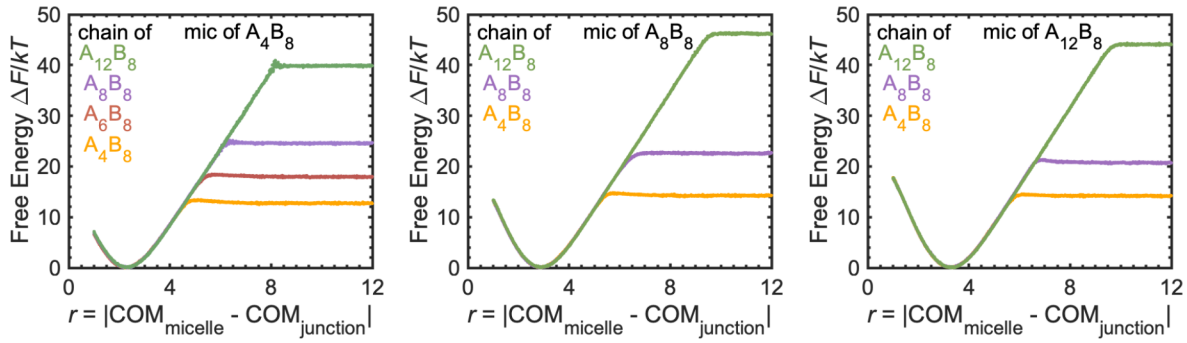

Figure 1. Free energy profiles of chain expulsion for a single chain of A_xB_8 from a micelle of (a) A_4B_8, (b) A_8B_8, and (c) $A_{12}B_8$ chains with $Q = 36$ as a function of the distance between the center-of-mass of the micelle and the AB junction of the chain being expelled (r).

events occurred. The value of the reaction coordinate was calculated every 10^3 time steps, and a histogram of r was constructed. This procedure was repeated for a set of values for r, yielding a series of neighboring umbrella windows with information about all observed values of the reaction coordinate (see Figure S1). $\Delta F_{original}$, i.e., the free energy profile for chain expulsion, was extracted by applying the weighted histogram analysis method (WHAM),[57,58] and the increased entropy due to the radial shell was subtracted as follows:[50]

$$\Delta F = \Delta F_{original} + kT \ln(r^2) \quad (5)$$

to yield a constant free energy once the chain is fully expelled from the micelle.[50] Error analysis was performed by bootstrapping.

RESULTS AND DISCUSSION

To analyze the effect of N_{core} on the free energy barrier at a fixed micelle size, the tracer chain length A_yB_8 was varied independent of the block length A_xB_8 of other chains in the micelle. The free energy trajectory of the expulsion of a tracer chain of length A_yB_8 from a micelle consisting of chains of A_4B_8 is shown in Figure 1a. Here, the total number of chains in the micelle, including the single chain of A_yB_8, is $Q = 36$. The reference (zero) free energy state is chosen to be the equilibrium position of the reaction coordinate, $r = 2.35$, where the chain junction lies at the core−corona interface (i.e., the micelle core radius). As the AB junction departs from the core−corona interface there is an increase in the free energy due to the introduction of unfavorable contacts; below the equilibrium r, the corona block is pulled into the core, and the unfavorable interactions between the core block and the corona block increase. Analogously, as r is increased from its equilibrium position, the unfavorable interactions between the core and the corona blocks increase as well as between the core block and the solvent. Beyond the point of highest free energy, defining the barrier to expulsion, there is a slight decrease in the free energy due to entropic relief as the chain leaves the crowded corona.

From Figure 1, increasing the core block length of the tracer chain consistently yields an increased free energy barrier for escape, as expected due to the increased energy penalty for expelling a longer core block. Importantly, in each case as the reaction coordinate is increased, the system follows the same free energy trajectory up to the r-position of the maximum free energy barrier. This effect of the tracer core block is reproducible for micelles of other sizes.

The free energy barriers from Figure 1 were then analyzed as a function of the tracer core block length. Figure 2

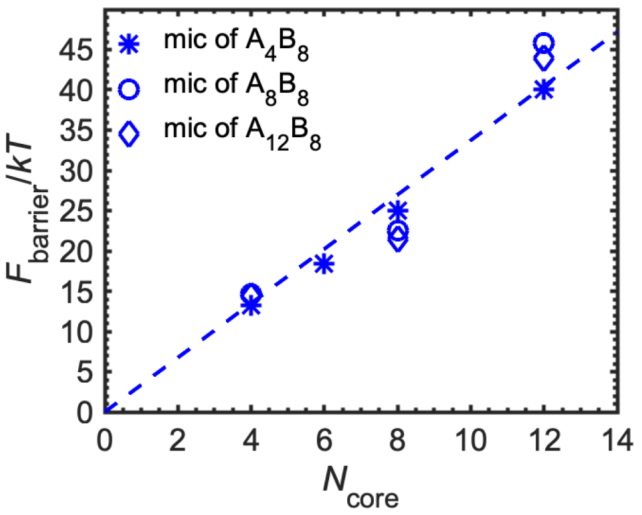

Figure 2. Free energy barrier to chain expulsion from an A_xB_8 micelle of $Q = 36$ as a function of the core block length N_{core} of the expelled chain.

demonstrates that $F_{barrier}$ is linear with N_{core} of the tracer chain. The free energy barriers from micelles of all sizes are included, as micelle size had a much more subtle effect on $F_{barrier}$ than N_{core} of the tracer chain. These results reproduce the scaling seen in past experiments[17,18,20] and simulations[42] of chain exchange in BCP micelle systems, rather than the $N_{core}^{2/3}$ scaling anticipated by Halperin and Alexander.[15] Notably, we observe this linear scaling despite differences in formation and equilibration conditions of the micelles used for simulations compared to experiment. Compared to past simulation work, we also use longer core block lengths ($N_{core} = 2-4$ in the study by Li and Dormidontova).[42] Additionally, here the barrier is obtained directly from the umbrella sampling, rather than through an analytical fitting of chain correlation functions.

Notably, our smallest tracer chain, A_4B_8, with an expulsion barrier of ~13 k_BT is comparable to those observed in a recent experimental system from TR-SANS. Wang et al. computed the escape barrier for a series of poly(styrene)-*b*-poly(ethylene-*alt*-propylene) (PS-*b*-PEP) in mixtures of phenyldodecane (phd) and squalane (sql).[22] For a system of 42 kDa PS and 64 kDa PEP in 25 vol % phd/75 vol % sql, $F_{barrier}$ was calculated as 15.1 k_BT. This system formed micelles of $R_{core} = 10.9$ nm and $R_h = 35$ nm, with $\chi = 1.46$. While being far from a rigorous

https://doi.org/10.1021/acs.macromol.2c01742
Macromolecules XXXX, XXX, XXX−XXX

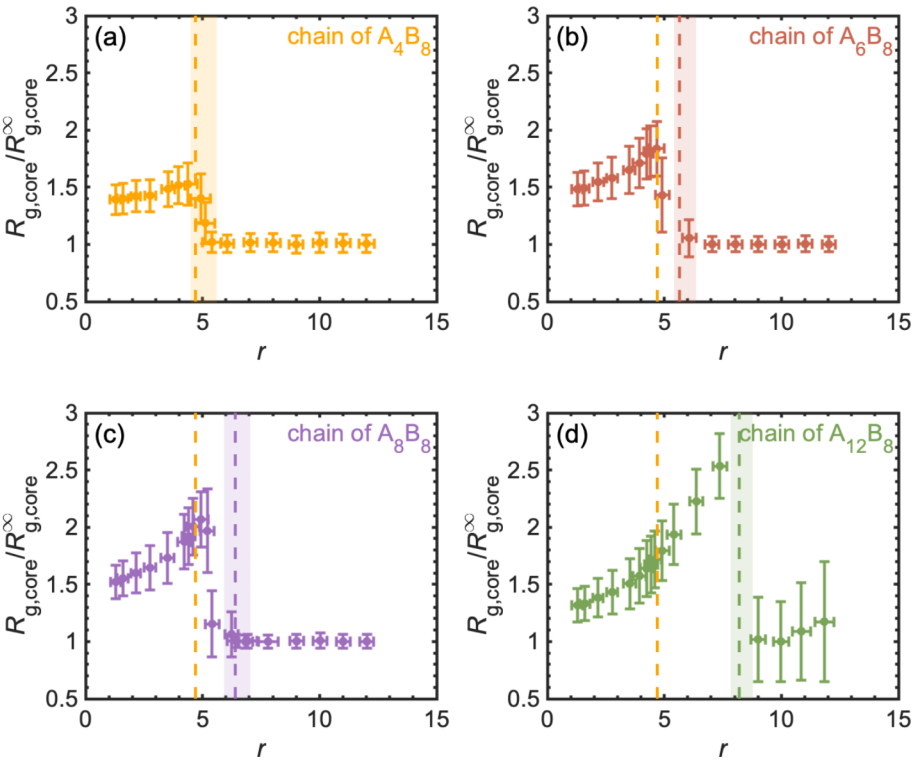

Figure 3. Radius of gyration of the core block along the reaction coordinate for expulsion for a chain of (a) A_4B_8, (b) A_6B_8, (c) A_8B_8, or (d) $A_{12}B_8$ from a micelle of A_4B_8 chains with $Q = 36$. Each point represents one umbrella window, and error bars are the standard deviation for observations over the course of the umbrella sample. The dashed lines represent the position of the transition state, defined by the point of highest free energy, for each case of A_yB_8, and the shaded area indicates its uncertainty. The dashed orange line indicating the position of the transition state for the A_4B_8 case is shown for all cases for comparison.

comparison with experiment, this provides a concrete example of an experimental system that has similar exchange barriers to the simulated system.

To understand the mechanistic basis behind the linear scaling of $F_{barrier}$ with N_{core}, the radius of gyration of the expelled core block, $R_{g,core}$, was analyzed as a function of the reaction coordinate for each tracer chain. Initially, close to the equilibrium position, Figure 3 shows that $R_{g,core}/R^{\infty}_{g,core} \approx 1.5$, indicating that the core block is significantly more expanded in the micelle core than after being expelled into a bad solvent. As the chain junction is pulled further from its favored position into the crowded corona, $R_{g,core}$ actually increases and the core block is stretched. This stretching persists with increasing r up to the transition state, whose r position is indicated by the vertical dashed line, where the core block remains at least partially extended. Importantly, the position of the transition state (and maximum $R_{g,core}$) occurs at larger values of r with increasing N_{core}, as the total extension of a longer core block can be greater before it becomes favorable for the chain to be fully expelled. This increase in $R_{g,core}$ toward the transition state occurs because the core beads furthest from the junction prefer to remain in the micelle core to shield them from the unfavorable interactions with the solvent and corona. Eventually, though, this partial stretching of the core block to minimize unfavorable core−corona contacts becomes unfavorable relative to completely expelling the chain from the micelle core, and $R_{g,core}$ decreases as the chain is expelled. Interestingly, the average $R_{g,core}$ does in many cases begin to decrease for the umbrella window where the r-position is below that of the transition state, accompanied by an increase in the variance of $R_{g,core}$, an observation that will be explained later in our discussion.

In contrast to what is observed in Figure 3, the Halperin and Alexander[15] model predicts that $R_{g,core}$ will steadily *decrease* with increasing r until the core block fully exits the micelle core, as a "budding" globule is forming from the expelled portion of the core block. We expect that if the Halperin and Alexander model were valid for the BCP systems, it would apply to even more strongly segregated systems than those in these simulations, where there is a larger internal energy penalty for core−solvent contacts and the core block has more incentive to immediately form a globule as it exits the core and enters the solvated corona. However, for the relatively strong segregation in these simulations, there is no evidence of core block collapse before or even at the transition state. We note that an $N_{core} = 4$−12 is too short to fully collapse to form a globule, based on past DPD studies;[59] however, the results in Figure 3 indicate that increasing N_{core} exacerbates the chain stretching at the transition state, rather than tending toward the postulated globular state.

To investigate the effect of micelle size, we monitored the dependence of the free energy profile on the lengths of the chains constituting the micelle. Thus, the core block lengths of the 35 A_xB_8 chains forming the micelle were varied, keeping the length of the tracer A_8B_8 chain constant. As seen in Figure 4, the equilibrium r increases with N_{core} of the chains forming the micelle, as the core radius of the micelle increases. Similarly, the position of the barrier shifts to larger r and in fact occurs at nearly the same r relative to the minimum free energy state. The free energy barrier to expulsion has a smaller dependence on the micelle core block length compared to the

https://doi.org/10.1021/acs.macromol.2c01742
Macromolecules XXXX, XXX, XXX−XXX

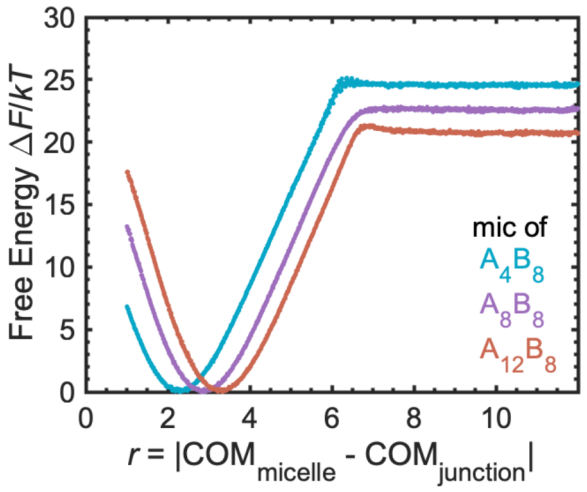

Figure 4. Free energy profiles of chain expulsion for a single chain of A_8B_8 from a micelle of A_xB_8 chains with $Q = 36$ as a function of the distance between the center-of-mass of the micelle and the AB junction of the chain being expelled (r).

tracer chain and is not proportional to N_{core} of the chains in the micelle. Here, we find the barrier for expulsion is smaller for an A_8B_8 chain expelled from a micelle consisting of longer core block chains; this may be due to less coronal crowding in micelles with larger cores as the corona block lengths were held constant. Notably, the increase in free energy upon expulsion for a given tracer chain varies depending on the micelle the tracer chain is expelled from. We expect that this is due to differences between the reference state in each case; the micelle consisting of chains with the shortest core block length, A_4B_8, is closest to its optimal aggregation number, and it takes more energy to expel a chain from this micelle. This effect of micelle core block length is subtle and is not significant for other tracer core block lengths (see Figures S2−S4 for other tracer chain lengths).

$R_{g,core}$ was computed for each umbrella window, and Figure 5 shows $R_{g,core}$ for an A_8B_8 tracer chain from micelles consisting of chains with various N_{core} from Figure 4. For each micelle N_{core}, the highest $R_{g,core}$ occurs close to the transition state marked by the dashed lines and close to the same distance from the core radius of the micelle. Effectively, we find that the size of the micelle has no effect on the extent of chain stretching at the transition state, and the position of the transition state does not change with respect to the core radius. Thus, the degree of extension of the core block at the transition state is independent of the micelle size.

To further resolve the conformation of the core block, we examined the distance between the micelle core and the terminal bead of the expelled chain, i.e., that furthest from the chain junction. This quantity was designated r_{first} and is displayed in Figure 6 for a series of subsequent umbrella windows for an A_8B_8 tracer chain expelled from a micelle formed of A_8B_8 chains. Initially, the bead furthest from the junction remains in the micelle core, even when the umbrella sampling bias is applied to hold the junction significantly outside of the micelle core, as seen in Figure 6b. As the position of biasing increases to larger r, we see a small population in which the first bead has exited the micelle core and fluctuates around the position of the umbrella window. As the bias position increases further, the fraction of states in which the first bead has exited the core increases, and in Figure 6d at the transition state this proportion is approximately half. This is characteristic of the transition states in all cases, as shown in Figure S5. As the bias is applied to hold the junction even further from the micelle core, the chain has fully exited the core, and the population of states in which the chain remains partially in the core decreases until it decays to zero in Figure 6f.

Importantly, the first bead either remains inside the core or escapes it completely when the penalty of stretching to minimize unfavorable internal energy considerations becomes too high. At the transition state, the core block goes from an extended conformation where the beads furthest from the junction remain in the core to a collapsed state as the chain is fully expelled. This also explains the decrease in $R_{g,core}$ prior to the transition state in Figure 3; as the core block begins to toggle between its stretched conformation and the collapsed state in which the chain fully exits the micelle core, the average $R_{g,core}$ decreases and its variance increases. This core block stretching at the transition state results in a linear dependence of the free energy barrier on N_{core}, thereby reproducing the experimental result. We show a schematic of the proposed transition state compared to the Halperin and Alexander mechanism in Figure 7.

MODEL

To describe the chain expulsion trajectory, we formulate a simple model. The reaction coordinate for umbrella sampling fixes the AB junction point at a distance r from the center-of-mass of the micelle. We assume that the micelle is spherical

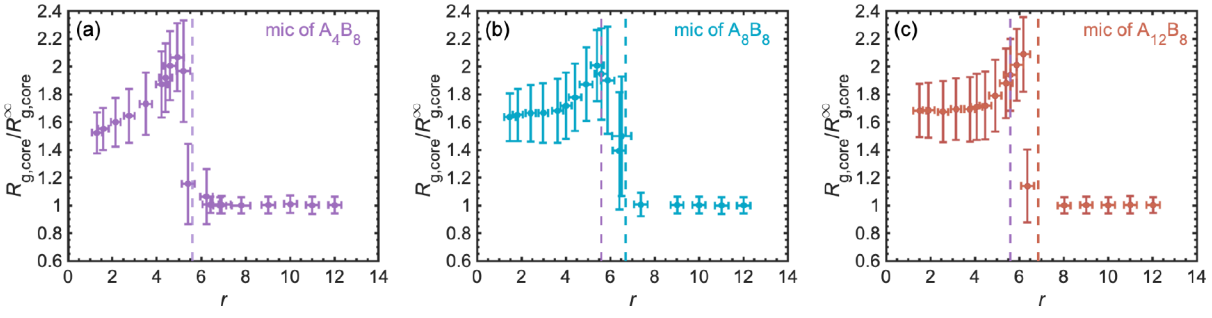

Figure 5. Radius of gyration of the core block along the reaction coordinate for expulsion for a chain of A_8B_8 from a micelle (a) A_4B_8, (b) A_8B_8, or (c) $A_{12}B_8$ chains of $Q = 36$. Each point represents one umbrella window, and error bars are the standard deviation for observations over the course of the umbrella sample. The dashed lines represent the position of the transition state for the escape of the A_8B_8 chain from a micelle consisting of A_xB_8 chains.

https://doi.org/10.1021/acs.macromol.2c01742
Macromolecules XXXX, XXX, XXX−XXX

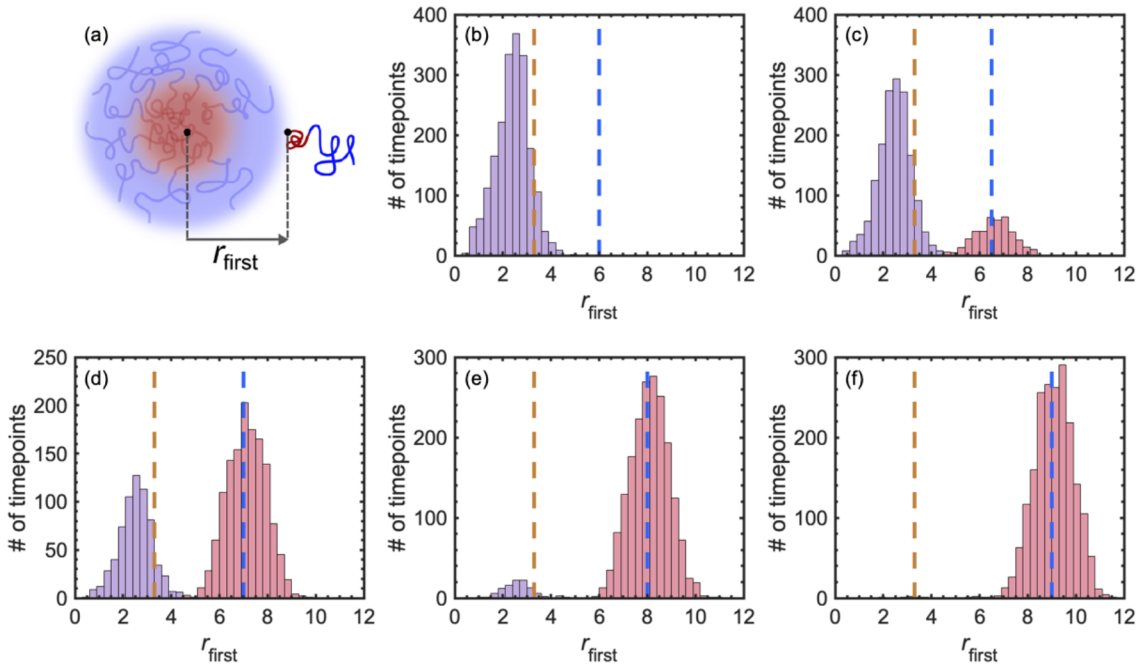

Figure 6. Distances of the "first bead" of the expelled chain for varying umbrella windows for an A_8B_8 chain expelled from a micelle of A_8B_8 chains with $Q = 36$. (a) Schematic of r_{first}, the distance from the micelle center of mass to the bead furthest from the chain junction. (b–f) Histograms of r_{first} for umbrella windows with centers at (b) 6.0, (c) 6.5, (d) 7.0 (the transition state), (e) 8.0, and (f) 9.0 (when the chain is full expelled from the micelle). The purple histogram represents the population of states in which the first bead is still in the micelle core, and the pink histogram the states in which the first bead has exited the micelle core. The core radius is marked by the dashed orange line, and the position of the bias on the chain junction is marked by the blue line.

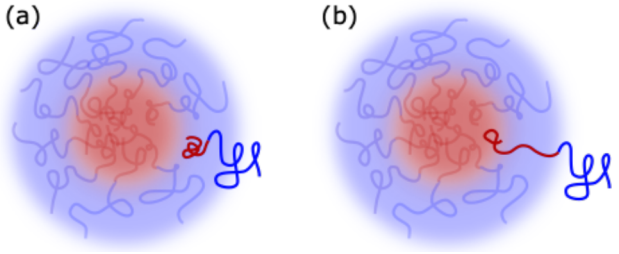

Figure 7. Transition states to chain expulsion: (a) the assumed globular transition state by Halperin and Alexander;[15] (b) the transition state observed in our system.

with a core radius of r_c. The test chain has a core block degree of polymerization N_{core}, with a fraction f of that block extracted from the micelle core when the AB junction is constrained to a position r. At the scaling level of approximation, the free energy cost due to extracting fN_{core} monomers from the micelle core into the corona/solvent with the AB junction point at position r is a balance between the unfavorable effect of A/B contact energy and stretching of the extracted core block monomers

$$\frac{F}{k_BT} \cong fN_{core}\Delta a + \frac{(r - r_c)^2}{fN_{core}b^2} \quad (6)$$

where Δa is the enthalpic cost per segment for bringing a core block into the corona/solvent and b is the statistical segment length of the core block.

For a given position r near the transition state, the fraction of the core block extracted minimizes the free energy.

$$\frac{\partial}{\partial f}\left(\frac{F}{k_BT}\right) = N_{core}\Delta a - \frac{(r - r_c)^2}{f^2 N_{core}b^2} = 0 \quad (7)$$

This extremum is a minimum in the free energy because the second derivative is positive. Solving for f gives

$$f \sim \frac{r - r_c}{N_{core}b(\Delta a)^{1/2}} \quad (8)$$

To determine the value of the free energy at some value of r, we substitute eq 8 into eq 6, which gives a free energy that is linear in $r - r_c$ and independent of N_{core}.

$$\frac{F}{k_BT} \cong \frac{r - r_c}{b}(\Delta a)^{1/2} \quad (9)$$

The free energy will keep increasing until it is more favorable to extract the entire core block into the solvent rather than stretch further. Assuming that the core block is wetted by the solvent, the maximum in the free energy is

$$\frac{F_{barrier}}{k_BT} \cong N_{core}\Delta a \quad (10)$$

and the free energy barrier is linear with both N_{core} and Δa, as seen in previous work.[38] The corresponding location r^* of the chain junction at the maximum in the free energy is obtained by equating eqs 9 and 10:

$$(r^* - r_c) \sim N_{core}b(\Delta a)^{1/2} \quad (11)$$

The key prediction of this model is already evident in Figure 1; for a micelle formed by chains of a given size A_xB_8, the free energy for extracting a tracer chain of size A_yB_8 should follow a similar trajectory with r, independent of the value of y, until reaching the point at which that core block size is fully

https://doi.org/10.1021/acs.macromol.2c01742
Macromolecules XXXX, XXX, XXX−XXX

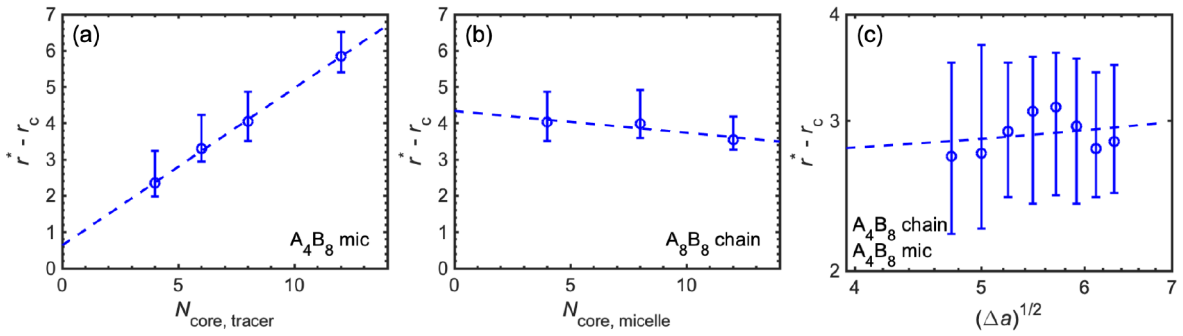

Figure 8. Dependence of $r^* - r_c$ on (a) the core block length of the tracer chain from micelles consisting of A_4B_8 chains, (b) the core block length of chains formulating the micelle, using a tracer chain of A_8B_8, and (c) the DPD excess interaction energy for A/B contacts, using data from Seeger et al.[38] Error bars are constructed using the error in the positions of r_c and r^* determined by bootstrapping.

f8 extracted. The related predictions for the dependence of the transition state are tested in Figure 8. Here, $r^* - r_c$ is determined by taking the difference of r^* determined by the position of highest free energy and r_c from the minimum free energy state; however, different ways to identify the position of transition state would lead to slightly different locations of the barrier.

Clearly, Figure 8a indicates that the radial distance of the transition state from the core radius of the micelle, $r^* - r_c$, varies linearly with N_{core} of the tracer chain, consistent with eq 11. Differences in the value of x for the micelle the tracer chain is expelled from are not explicitly included in the theory. In Figure 8b, the transition state occurs at approximately the same distance from the micelle core regardless of the micelle size and is within the uncertainty of the peak position. This result indicates that the base micelle has, at most, a small effect on the expulsion trajectory of the tracer chain.

In Figure 8c, the position of the transition state was recorded for a range of values of DPD excess interaction energy Δa from previous work.[38] Contrary to the model, which predicts the position of the transition state to vary linearly with $(\Delta a)^{1/2}$, the dependence on Δa appears to be weakly nonmonotonic in the range of values tested. At the highest values of Δa, the decrease in $r^* - r_c$ may be due to the observed deformation of the micelle cores at the transition state[38] due to the large internal energy penalty for exposure of core monomers to the corona/solvent. However, we note that the changes in the position of the transition state in this range of Δa are likely not significant and well within the range of error for the data.

The fraction of the core block extracted from the micelle core, f, was computed for each umbrella window using a distance criterion of $1.0d_p$ from other monomers forming the micelle core. Here, the tracer chain of $N_{core} = 12$ is used to minimize effects of discretizing the number of core beads.
f9 Initially, Figure 9 shows that $f = 0$ as all monomers are within the micelle core, and past the transition state f rapidly increases to unity as the chain is fully expelled from the micelle core. In the vicinity of the transition state, f increases linearly with distance from the micelle core, as predicted by eq 8. Notably, the model captures this observed scaling behavior despite there being relatively few assumptions beyond the conformation of the core block of the expelled chain around the transition state.

SUMMARY

We explored the effect of increasing the core block length on the barrier to chain expulsion using a tracer chain in a micelle consisting of either the same, or different, chains. Compared to the A_4B_8 case, using a tracer core block of up to 12 beads yields a larger free energy barrier to expulsion and a transition state where the chain junction is further from the micelle center-of-mass, along with increased core block stretching toward the transition state. In addition, using a tracer chain of constant core block length, changing the core block length of other chains in the micelle does not change the observed transition state or the extent of core block stretching. Overall, the observed transition state, where the core chain stretches to allow some core beads to remain in the core to minimize unfavorable contacts, persists for longer chain lengths, and the transition state for the expelled chain appears to be independent of the matrix. We present a model based on this proposed mechanism and show that the simulation data are consistent with its implicit scaling behavior. Interestingly, the proposed mechanism provides a possible explanation for the experimental observations, which show that the free energy barrier to chain exchange increases linearly with core block length.

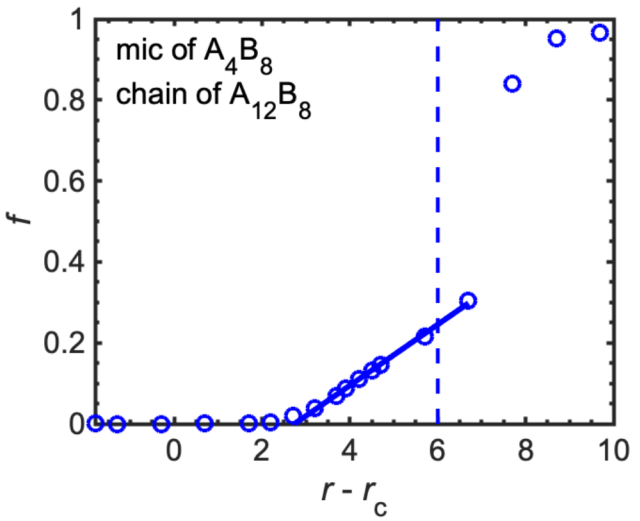

Figure 9. Fraction of expelled core beads as a function of radial distance of the chain junction from the micelle core radius. The dashed line indicates the position of the transition state.

ASSOCIATED CONTENT

Supporting Information

The Supporting Information is available free of charge at https://pubs.acs.org/doi/10.1021/acs.macromol.2c01742.

https://doi.org/10.1021/acs.macromol.2c01742
Macromolecules XXXX, XXX, XXX−XXX

Example histograms of observed values of the reaction coordinate for a series of umbrella windows, free energy profiles of chain expulsion of single chains of fixed core block length (A_4B_8, A_6B_8, and $A_{12}B_8$) from micelles of various core block lengths, histograms of "first bead" positions at the transition states for varying core block lengths of both the tracer chain and micelle chains (PDF)

AUTHOR INFORMATION

Corresponding Authors

Kevin D. Dorfman − *Department of Chemical Engineering and Materials Science, University of Minnesota—Twin Cities, Minneapolis, Minnesota 55455, United States;* orcid.org/0000-0003-0065-5157; Email: dorfman@umn.edu

Timothy P. Lodge − *Department of Chemical Engineering and Materials Science and Department of Chemistry, University of Minnesota—Twin Cities, Minneapolis, Minnesota 55455, United States;* orcid.org/0000-0001-5916-8834; Email: lodge@umn.edu

Author

Sarah C. Seeger − *Department of Chemical Engineering and Materials Science, University of Minnesota—Twin Cities, Minneapolis, Minnesota 55455, United States;* orcid.org/0000-0002-3224-7222

Complete contact information is available at: https://pubs.acs.org/10.1021/acs.macromol.2c01742

Notes

The authors declare no competing financial interest.

ACKNOWLEDGMENTS

We acknowledge Vaidyanathan Sethuraman for helpful discussions about the techniques used in this work. This material was supported by the National Science Foundation Polymers Program (DMR-2103630) and by an NSF Graduate Research Fellowship (S.C.S.). Simulations were conducted on the Minnesota Supercomputing Institute (MSI) at the University of Minnesota.

REFERENCES

(1) Lohmuller, T.; Aydin, D.; Schwieder, M.; Morhard, C.; Louban, I.; Pacholski, C.; Spatz, J. P. Nanopatterning by Block Copolymer Micelle Nanolithography and Bioinspired Applications. *Biointerphases* **2011**, *6* (1), MR1−MR12.

(2) Glass, R.; Möller, M.; Spatz, J. P. Block Copolymer Micelle Nanolithography. *Nanotechnology* **2003**, *14*, 1153−1160.

(3) Cotanda, P.; Lu, A.; Patterson, J. P.; Petzetakis, N.; O'Reilly, R. K. Functionalized Organocatalytic Nanoreactors: Hydrophobic Pockets for Acylation Reactions in Water. *Macromolecules* **2012**, *45*, 2377−2384.

(4) Anderson, W. *Block Copolymers as Viscosity Index Improvers for Lubrication Oils* **1973**, 3763044.

(5) Stambaugh, R. L.; Kinker, B. G. Viscosity Index Improvers and Thickeners BT. In *Chemistry and Technology of Lubricants*; Mortier, R. M., Fox, M. F., Orszulik, S. T., Eds.; Springer: Dordrecht, the Netherlands, 2010; pp 153−187.

(6) Hubbell, J. A. Enhancing Drug Function. *Science* **2003**, *300* (5619), 595−596.

(7) Kazunori, K.; Glenn, S. K.; Masayuki, Y.; Teruo, O.; Yasuhisa, S. Block Copolymer Micelles as Vehicles for Drug Delivery. *J. Controlled Release* **1993**, *24* (1−3), 119−132.

(8) Luo, L.; Tam, J.; Maysinger, D.; Eisenberg, A. Cellular Internalization of Poly(Ethylene Oxide)-*b*-Poly(ε-Caprolactone) Diblock Copolymer Micelles. *Bioconjugate Chem.* **2002**, *13* (6), 1259−1265.

(9) Kim, S.; Shi, Y.; Kim, J. Y.; Park, K.; Cheng, J. Overcoming the Barriers in Micellar Drug Delivery: Loading Efficiency, *in vivo* Stability, and Micelle−Cell Interaction. *Expert Opin. Drug Delivery* **2010**, *7* (1), 49−62.

(10) Lodge, T. P.; Seitzinger, C. L.; Seeger, S. C.; Yang, S.; Gupta, S.; Dorfman, K. D. Dynamics and Equilibration Mechanisms in Block Copolymer Particles. *ACS Polym. Au* (in press, DOI: 10.1021/acspolymersau.2c00033).

(11) Aniansson, E. A. G.; Wall, S. N.; Almgren, M.; Hoffmann, H.; Kielmann, I.; Ulbricht, W.; Zana, R.; Lang, J.; Tondre, C. Theory of the Kinetics of Micellar Equilibria and Quantitative Interpretation of Chemical Relaxation Studies of Micellar Solutions of Ionic Surfactants. *J. Phys. Chem.* **1976**, *80*, 905−922.

(12) Won, Y.-Y.; Davis, H. T.; Bates, F. S. Molecular Exchange in PEO−PB Micelles in Water. *Macromolecules* **2003**, *36* (3), 953−955.

(13) Zhao, D.; Ma, Y.; Lodge, T. P. Exchange Kinetics for a Single Block Copolymer in Micelles of Two Different Sizes. *Macromolecules* **2018**, *51* (6), 2312−2320.

(14) He, Y.; Li, Z.; Simone, P.; Lodge, T. P. Self-Assembly of Block Copolymer Micelles in an Ionic Liquid. *J. Am. Chem. Soc.* **2006**, *128* (8), 2745−2750.

(15) Halperin, A.; Alexander, S. Polymeric Micelles: Their Relaxation Kinetics. *Macromolecules* **1989**, *22* (5), 2403−2412.

(16) Dormidontova, E. E. Micellization Kinetics in Block Copolymer Solutions: Scaling Model. *Macromolecules* **1999**, *32* (22), 7630−7644.

(17) Choi, S.-H.; Bates, F. S.; Lodge, T. P. Molecular Exchange in Ordered Diblock Copolymer Micelles. *Macromolecules* **2011**, *44* (9), 3594−3604.

(18) Ma, Y.; Lodge, T. P. Chain Exchange Kinetics in Diblock Copolymer Micelles in Ionic Liquids: The Role of χ. *Macromolecules* **2016**, *49* (24), 9542−9552.

(19) Zhao, D.; Ma, Y.; Wang, E.; Lodge, T. P. Micellization of Binary Diblock Co-Polymer Mixtures in an Ionic Liquid. *Macromolecules* **2019**, *52* (12), 4729−4738.

(20) Lund, R.; Willner, L.; Pipich, V.; Grillo, I.; Lindner, P.; Colmenero, J.; Richter, D. Equilibrium Chain Exchange Kinetics of Diblock Copolymer Micelles: Effect of Morphology. *Macromolecules* **2011**, *44* (15), 6145−6154.

(21) Willner, L.; Poppe, A.; Allgaier, J.; Monkenbusch, M.; Richter, D. Time-resolved SANS for the Determination of Unimer Exchange Kinetics in Block Copolymer Micelles. *Europhys. Lett.* **2001**, *55*, 667.

(22) Wang, E.; Zhu, J.; Zhao, D.; Xie, S.; Bates, F. S.; Lodge, T. P. Effect of Solvent Selectivity on Chain Exchange Kinetics in Block Copolymer Micelles. *Macromolecules* **2020**, *53* (1), 417−426.

(23) Zhao, D.; Ma, Y.; Lodge, T. P. Exchange Kinetics for a Single Block Copolymer in Micelles of Two Different Sizes. *Macromolecules* **2018**, *51* (6), 2312−2320.

(24) Cooksey, T. J.; Singh, A.; Le, K. M.; Wang, S.; Kelley, E. G.; He, L.; Vajjala Kesava, S.; Gomez, E. D.; Kidd, B. E.; Madsen, L. A.; Robertson, M. L. Tuning Biocompatible Block Copolymer Micelles by Varying Solvent Composition: Core/Corona Structure and Solvent Uptake. *Macromolecules* **2017**, *50* (11), 4322−4334.

(25) Zinn, T.; Willner, L.; Lund, R.; Pipich, V.; Richter, D. Equilibrium Exchange Kinetics in N-Alkyl−PEO Polymeric Micelles: Single Exponential Relaxation and Chain Length Dependence. *Soft Matter* **2012**, *8* (3), 623−626.

(26) Lu, J.; Choi, S.; Bates, F. S.; Lodge, T. P. Molecular Exchange in Diblock Copolymer Micelles: Bimodal Distribution in Core-Block Molecular Weights. *ACS Macro Lett.* **2012**, *1* (8), 982−985.

(27) Lu, J.; Bates, F. S.; Lodge, T. P. Addition of Corona Block Homopolymer Retards Chain Exchange in Solutions of Block Copolymer Micelles. *Macromolecules* **2016**, *49* (4), 1405−1413.

(28) Kim, S.; Lee, S.; Choi, S.-H.; Char, K. Chain Exchange Kinetics of Bottlebrush Block Copolymer Micelles. *Macromolecules* **2021**, *54* (10), 4739−4746.

(29) Wang, Y.; Kausch, C. M.; Chun, M.; Quirk, R. P.; Mattice, W. L. Exchange of Chains between Micelles of Labeled Polystyrene-Block-Poly(Oxyethylene) As Monitored by Nonradiative Singlet Energy Transfer. *Macromolecules* **1995**, *28* (4), 904−911.
(30) Prochazka, K.; Bednar, B.; Mukhtar, E.; Svoboda, P.; Trnena, J.; Almgren, M. Nonradiative Energy Transfer in Block Copolymer Micelles. *J. Phys. Chem.* **1991**, *95* (11), 4563−4568.
(31) Creutz, S.; van Stam, J.; Antoun, S.; De Schryver, F. C.; Jerome, R. Exchange of Polymer Molecules between Block Copolymer Micelles Studied by Emission Spectroscopy. A Method for the Quantification of Unimer Exchange Rates. *Macromolecules* **1997**, *30* (14), 4078−4083.
(32) Cao, T.; Munk, P.; Ramireddy, C.; Tuzar, Z.; Webber, S. E. Fluorescence Studies of Amphiphilic Poly(Methacrylic Acid)-Block-Polystyrene-Block-Poly(Methacrylic Acid) Micelles. *Macromolecules* **1991**, *24* (23), 6300−6305.
(33) Smith, C. K.; Liu, G. Determination of the Rate Constant for Chain Insertion into Poly(Methyl Methacrylate)-*Block*-Poly-(Methacrylic Acid) Micelles by a Fluorescence Method. *Macromolecules* **1996**, *29* (6), 2060−2067.
(34) Wang, Y.; Kausch, C. M.; Chun, M.; Quirk, R. P.; Mattice, W. L. Exchange of Chains between Micelles of Labeled Polystyrene-Block-Poly(Oxyethylene) As Monitored by Nonradiative Singlet Energy Transfer. *Macromolecules* **1995**, *28* (4), 904−911.
(35) Cavicchi, K. A.; Lodge, T. P. Self-Diffusion and Tracer Diffusion in Sphere-Forming Block Copolymers. *Macromolecules* **2003**, *36*, 7158−7164.
(36) Yokoyama, H.; Kramer, E. J. Self-diffusion of Asymmetric Diblock Copolymers with a Spherical Domain Structure. *Macromolecules* **1998**, *31*, 7871−7876.
(37) Yokoyama, H.; Kramer, E. J. Diffusion of Triblock Copolymers in a Spherical Domain Structure. *Macromolecules* **2000**, *33*, 954−959.
(38) Seeger, S. C.; Dorfman, K. D.; Lodge, T. P. Free Energy Trajectory for Escape of a Single Chain from a Diblock Copolymer Micelle. *ACS Macro Lett.* **2021**, *10* (12), 1570−1575.
(39) Español, P.; Warren, P. Statistical Mechanics of Dissipative Particle Dynamics. *Europhys. Lett.* **1995**, *30* (4), 191−196.
(40) Groot, R. D.; Warren, P. B. Dissipative Particle Dynamics: Bridging the Gap between Atomistic and Mesoscopic Simulation. *J. Chem. Phys.* **1997**, *107* (11), 4423−4435.
(41) Li, Z.; Dormidontova, E. E. Kinetics of Diblock Copolymer Micellization by Dissipative Particle Dynamics. *Macromolecules* **2010**, *43* (7), 3521−3531.
(42) Li, Z.; Dormidontova, E. E. Equilibrium Chain Exchange Kinetics in Block Copolymer Micelle Solutions by Dissipative Particle Dynamics Simulations. *Soft Matter* **2011**, *7* (9), 4179.
(43) Peters, A. J.; Lodge, T. P. Chain Exchange Kinetics of Asymmetric B_1AB_2 Linear Triblock and AB_1B_2 Branched Triblock Copolymers. *Macromolecules* **2017**, *50* (16), 6303−6313.
(44) Prhashanna, A.; Khan, S. A.; Chen, S. B. Kinetics of Chain Exchange between Diblock Copolymer Micelles. *Macromol. Theory Simul.* **2016**, *25*, 383−391.
(45) Prhashanna, A.; Chen, S. B. Chain Exchange Kinetics between Linear ABA-Type Triblock Copolymer Micelles. *Polymer* **2017**, *118*, 22−29.
(46) Prhashanna, A.; Dormidontova, E. E. Tadpole and Mixed Linear/Tadpole Micelles of Diblock Copolymers: Thermodynamics and Chain Exchange Kinetics. *Macromolecules* **2017**, *50* (4), 1740−1748.
(47) Prhashanna, A.; Dormidontova, E. E. Micelle Self-Assembly and Chain Exchange Kinetics of Tadpole Block Copolymers with a Cyclic Corona Block. *Macromolecules* **2020**, *53* (3), 982−991.
(48) Torrie, G. M.; Valleau, J. P. Nonphysical sampling distributions in Monte Carlo free-energy estimation: Umbrella sampling. *J. Comput. Phys.* **1977**, *23* (2), 187−199.
(49) von Gottberg, F. K.; Smith, K. A.; Hatton, T. A. Dynamics of Self-Assembled Surfactant Systems. *J. Chem. Phys.* **1998**, *108* (5), 2232−2244.
(50) Yuan, F.; Wang, S.; Larson, R. G. Potentials of Mean Force and Escape Times of Surfactants from Micelles and Hydrophobic Surfaces Using Molecular Dynamics Simulations. *Langmuir* **2015**, *31* (4), 1336−1343.
(51) Wen, B.; Bai, B.; Larson, R. G. Surfactant Desorption and Scission Free Energies for Cylindrical and Spherical Micelles from Umbrella-Sampling Molecular Dynamics Simulations. *J. Colloid Interface Sci.* **2021**, *599*, 773−784.
(52) Helfand, E. Diffusion in Strongly Segregated Block Copolymers. *Macromolecules* **1992**, *25* (1), 492−493.
(53) Underhill, R. S.; Ding, J.; Birss, V. I.; Liu, G. Chain Exchange Kinetics of Polystyrene- *Block* -Poly(2-Cinnamoylethyl Methacrylate) Micelles in THF/Cyclopentane Mixtures. *Macromolecules* **1997**, *30* (26), 8298−8303.
(54) Zinn, T.; Willner, L.; Lund, R.; Pipich, V.; Richter, D. Molecular Exchange Kinetics of Micelles: Corona Chain Length Dependence. *ACS Macro Lett.* **2016**, *5* (7), 884−888.
(55) Wang, E.; Lu, J.; Bates, F. S.; Lodge, T. P. Effect of Corona Block Length on the Structure and Chain Exchange Kinetics of Block Copolymer Micelles. *Macromolecules* **2018**, *51* (10), 3563−3571.
(56) Plimpton, S. Fast Parallel Algorithms for Short-Range Molecular Dynamics. *J. Comput. Phys.* **1995**, *117* (1), 1−19.
(57) Grossfield, A. An Implementation of WHAM: The Weighted Histogram Analysis Method Version 2.0.10. 20.
(58) Kumar, S.; Rosenberg, J. M.; Bouzida, D.; Swendsen, R. H.; Kollman, P. A. The Weighted Histogram Analysis Method for Free-Energy Calculations on Biomolecules. I. The Method. *J. Comput. Chem.* **1992**, *13* (8), 1011−1021.
(59) Guo, J.; Liang, H.; Wang, Z. Coil-to-globule transition by dissipative particle dynamics simulation. *J. Chem. Phys.* **2011**, *134*, 244904.

https://doi.org/10.1021/acs.macromol.2c01742
Macromolecules XXXX, XXX, XXX−XXX